Hindawi
International Journal of Photoenergy
Volume 2022, Article ID 7303034, 9 pages
https://doi.org/10.1155/2022/7303034

Research Article

Dibenzo[b,f][1,5]Diazocines/ZnO Organic/Inorganic Hybrid Photoanodes for Efficient Photo Electrochemical Water Splitting

Sissembayeva Yana,[1] Soo Kyung Cho,[2] and Yoon-Hwae Hwang[1]

[1]*Department of Nano Energy Engineering and BK 21 PLUS Nanoconvergence Technology, Pusan National University, Miryang 50463, Republic of Korea*
[2]*Crystal Bank, Pusan National University, Miryang 50463, Republic of Korea*

Correspondence should be addressed to Yoon-Hwae Hwang; yhwang@pusan.ac.kr

Received 29 July 2022; Revised 18 November 2022; Accepted 1 December 2022; Published 23 December 2022

Academic Editor: Fayaz Hussain

In this study, we propose dibenzo[b,f][1,5]diazocine/ZnO organic/inorganic hybrid photoanode for application in the photoelectrochemical water splitting. The electrode consisting of inorganic ZnO nanorod (ZnO NR) array structures and organic diazocine derivative film with or without platinum nanoparticle (Pt NP) cocatalyst was examined. The morphology characterization was performed by FESEM. UV-vis absorbance spectra showed enhanced absorbance in the visible light spectrum for the hybrid sample. Photoluminescence analysis of a hybrid sample showed a significant decrease in charge recombination and enhanced charge separation. Photoelectrochemical measurements revealed an increase in current density for the organic/inorganic hybrid photoanode reaching 1.256 mA/cm^2 at 1.23 V vs. RHE which is almost two times higher than bare ZnO NR arrays (0.716 mA/cm^2 at 1.23 V vs. RHE). The addition of the Pt NP cocatalyst further enhanced the photocurrent density up to 1.636 mA/cm^2. Therefore, proposed organic/inorganic hybrid photoelectrode is a promising candidate for the efficient solar water splitting.

1. Introduction

Energy crisis is a major worldwide issue which is being actively pursued by countless researchers. A solar water splitting is one of the promising technologies towards sustainable energy generation through direct conversion of water and sunlight to electrical current and hydrogen gas [1, 2]. Upon the illumination of photoelectrode with sunlight, an electron is excited from the valence band to the conduction band and is used for current generation in redox reactions followed by hydrogen gas evolution. Solar water splitting was discovered by Fujishima and Honda in the early 1970s by the means of photoassisted electrochemical water oxidation on an n-type TiO_2 single crystal [3]. Ever since the photocatalytic and photoelectrochemical water splitting on semiconducting materials have been studied extensively [4–8].

Much research was conducted on the inorganic semiconducting materials such as WO_3, $BiVO_4$, and ZnO, and many showed promising efficiencies especially when heterojunction arrays are adopted [9–11]. However, inorganic materials often used in a water-splitting applications exhibit several disadvantages such as difficulty in tuning the innate properties such as bandgaps, relatively higher cost due to limited availability in nature, low structural tenability, and corrosion in electrolyte solutions [12–14]. Therefore, finding the right material remains a significant challenge in constructing an efficient solar-to-hydrogen (STH) conversion technology and implementing it on a large-scale basis.

The limitations of stand-alone inorganic semiconducting system can be resolved by introducing organic materials resulting in an organic-inorganic hybrid structure. Such hybrid system can benefit from the advantages of both organic and inorganic materials such as tunable bandgap, energy levels, and charge transport mobility while still exhibiting high efficiency [15]. Moreover, organic semiconducting materials can serve as photosensitizers that enhance the absorbance of the inorganic semiconducting photocatalysts

for photoelectrochemical (PEC) redox reactions [16]. Organic semiconductors can additionally be utilized as host materials for immobilizing the semiconductor nanostructures, therefore boosting the stability of hybrid photoelectrodes [17–19] or improving the chemical stability of the inorganic semiconductors from the aqueous environment [20–22]. Therefore, the development of a new class organic/inorganic hybrid semiconducting material for solar water splitting is in high demand as it makes it possible to synergize the advantages of organic and inorganic materials. As such, much research was conducted on the development of organic/inorganic hybrid photoelectrodes in search of the efficient water-splitting electrodes.

In this study, a dibenzo[b,f][1,5]diazocine derivative from substituted 2-aminobenzophenone was synthesized. The obtained material was applied as an organic film on the top of the inorganic ZnO nanorod (ZnO NR) array which was hydrothermally grown for 2 hours. The obtained hybrid photoelectrode was used as a photoanode for the oxygen evolution reaction of electrochemical water splitting. The self-assembly behavior of organic film to successfully make interfaces was characterized as well as chemical and physical properties of a hybrid semiconducting photoanode. Therefore, dibenzo[b,f][1,5]diazocine/ZnO organic/inorganic hybrid photoelectrode is proposed as a new class of semiconducting material with low cost, easy processing, optoelectronic tenability, and good stability for solar-driven water splitting.

2. Materials and Methods

2.1. Materials. FTO glass substrates were washed in acetone (99.5% purity), ethyl alcohol (95% purity) and deionized (DI) water. Hexamethylenetetramine (HMTA, ACS reagent, ≥99.0%, Sigma-Aldrich) and zinc nitrate hexahydrate (reagent grade, 98%, Sigma-Aldrich) were used for preparation of growth solution during hydrothermal synthesis of ZnO NR. Diazocine derivative ((5Z,11Z)-6,12-diphenyl-2,8-di((E)-styryl)-dibenzo[b,f][1,5]diazocine) was synthesized and characterized according to the previously published paper from our group [23]. Tetrahydrofuran (THF, anhydrous, contains 250 ppm butylated hydroxytoluene (BHT) as inhibitor, ≥99.9%, Sigma-Aldrich) was used as a solvent for organic material stock and film solutions. 0.45 μm PTFE-D syringe filter (Hyundai micro) was used for stock solution filtering before organic film preparation. 70 nm Pt nanoparticle (NP) suspension (0.05 mg/mL, citrate functionalized in 4 mM aqueous sodium citrate buffer, Sigma-Aldrich) was centrifuged using Nanosep centrifugal filter (Pall Corporation) and washed with ethyl alcohol (200 proof, anhydrous, ≥99.5%, Sigma-Aldrich) for preparation of diazocine film/ZnO NR/Pt sample. Sodium carbonate (powder, ACS reagent, ≥99.5%, Sigma-Aldrich) and sodium bicarbonate (powder, first grade reagent, ≥99.6%, Shinyo Pure Chemicals Co., Ltd.) were used for 0.05 M (pH = 10.5) carbonate buffer electrolyte preparation utilized in photoelectrochemical measurements.

2.2. Preparation of ZnO Inorganic Nanorod Structure. The FTO substrates 1×1 cm^2 in area were washed in acetone, ethanol, and DI water for 15 minutes each in a sonication bath, dried in a convection oven. ZnO films for the seed layer have been deposited on FTO substrate using a ZnO target by RF sputtering system. The FTO substrate was fixed inside the sputter chamber, and the chamber was evacuated to a pressure of less than 1.0×10^{-6} Torr by the turbomolecular pump. The concentrations of Ar and O_2 were controlled using a mass flow controller, and the pressure in the chamber was maintained at 5 mTorr. RF power at 13.56 MHz was 50 W, O_2 concentration was 15%. The ZnO film was deposited at 200 nm at a rate of 6 nm/min. After deposition, a hole array mask was formed by an electron beam lithography process on ZnO/FTO. The hole diameter and period of the structure were 500 nm and 2 μm, respectively.

The hydrothermal growth method was utilized to grow the ZnO NR on as obtained seed layers on FTO for 2 hours in 30 mM aqueous solutions of hexamethylenetetramine (HMTA, ACS reagent, ≥99.0%, Sigma-Aldrich) and zinc nitrate hexahydrate (reagent grade, 98%, Sigma-Aldrich). The samples were rinsed in ethanol and dried using a nitrogen blow.

2.3. Preparation of Organic/Inorganic Hybrid Structure. The diazocine film/ZnO NR hybrid sample was prepared as follows. To make an organic material stock solution, 0.05 g of diazocine film powder was dissolved in 1 mL of tetrahydrofuran (THF, anhydrous, contains 250 ppm BHT as inhibitor, ≥99.9%, Sigma-Aldrich). The obtained stock solution was filtered through the 0.45 μm PTFE-D syringe filter (Hyundai micro). To prepare the film solution used for the fabrication of hybrid samples, 100 μL of stock solution was added to the 900 μL of THF. The prepared solution was drop-casted twice on the as-prepared ZnO NR samples and dried at room temperature overnight prior to characterizations.

Pt nanoparticle/diazocine film/ZnO NR hybrid sample was prepared as follows. A 70 nm Pt NP suspension (0.05 mg/mL, citrate functionalized in 4 mM aqueous sodium citrate buffer, Sigma-Aldrich) was centrifuged for 5 minutes at 5000 rpm using Nanosep centrifugal filter (Pall Corporation). A 20 μL of pure ethyl alcohol (200 proof, anhydrous, ≥99.5%, Sigma-Aldrich) was used to wash the filter and transfer the NP into a tube, followed by the addition of 80 μL of THF. After the pipetting, 50 μL of Pt NP solution was added to 1 mL of diazocine film solution. The as-prepared solution was drop-casted twice on the ZnO NR samples.

2.4. Characterizations of Organic/Inorganic Hybrids. The morphology was characterized using a field-emission scanning electron microscope (FESEM, Hitachi S-4700) and energy dispersive X-ray spectroscopy (EDS) for elemental mapping analysis. UV-visible absorption spectra were analyzed using a UV-spectrophotometer (Evolution 220). The photoluminescence emission spectra were analyzed by photoluminescence spectra excited by a 266 nm laser. The photoelectrochemical measurements were conducted in a three-electrode system under simulated AM 1.5 (100 mW/cm^2) solar irradiation with a potentiostat (IviumStat, Ivium Technologies) in a 0.05 M carbonate buffer solution (pH = 10.5) with an Ag/AgCl reference electrode and a platinum mesh as a counter electrode. All measurements were performed at room

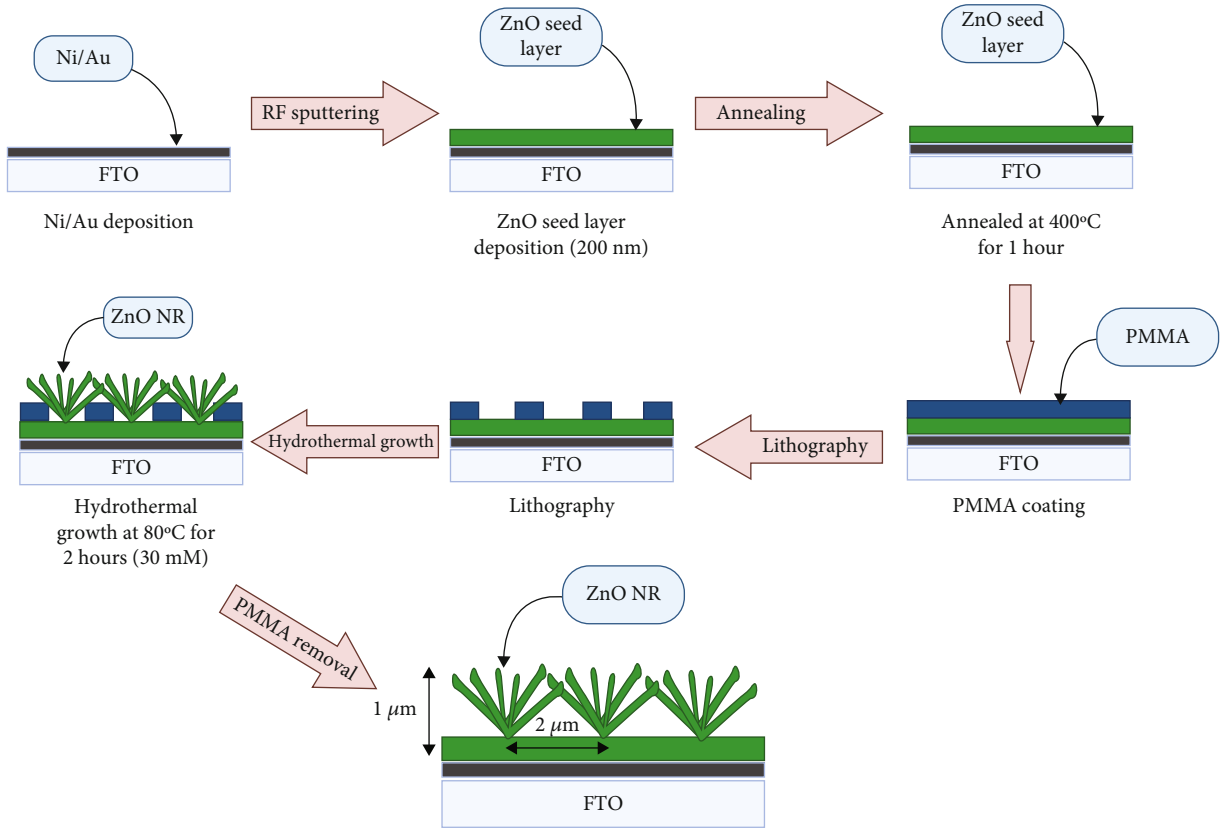

Figure 1: Schematics of inorganic ZnO nanorod layer preparation by combined lithography and hydrothermal growth.

temperature. The carbonate buffer was prepared using sodium carbonate (powder, ACS reagent, ≥99.5%, Sigma-Aldrich) and sodium bicarbonate (powder, first grade reagent, ≥99.6%, Shinyo Pure Chemicals Co., Ltd.) in DI water.

All linear-scanning voltammetry (LSV) curves were obtained by sweeping the potential with an E step of 10 mV and scan rate of 50 mV/s. The applied bias of the electrochemical measurements is converted to the potential relative to the reversible hydrogen electrode (RHE) using the Nernst equation:

$$\mathrm{E\,(RHE)} = \mathrm{E}\left(\frac{\mathrm{Ag}}{\mathrm{AgCl}}\right) + 0.0591\,\mathrm{pH} + 0.1976\,\mathrm{V}, \quad (1)$$

where $\mathrm{E}_{(\mathrm{Ag/AgCl})}$ is the applied bias relative to the Ag/AgCl reference electrode.

3. Results and Discussion

3.1. ZnO Inorganic Nanorod Structure. Figure 1 demonstrates the ZnO NR preparation procedure which involves the seed layer preparation and growth of ZnO NR using a hydrothermal method. As seen from the Figure 1, prior to RF sputtering, an Ni/Au layer was deposited for better adhesion of ZnO seeds to the substrate surface. The 200 nm ZnO seed layer deposition was followed by 1 hour annealing at 400°C to strengthen the microstructure. The PMMA was then coated on the seed layer as a starting step of electron-beam lithography process. After the mask formation, a hydrothermal growth was performed to grow the ZnO NR array for 2 hours at 80°C in 30 mM HMTA and zinc nitrate hexahydrate aqueous growth solutions. The resulting ZnO microstructures were rinsed with ethanol and dried by means of nitrogen blowing. The hole diameter and the distance between ZnO NR bundles were 500 nm and 2 μm, respectively. The final microstructure height was optimized to 1 μm in order to provide a better contact area (Figure 1).

3.2. Diazocine/ZnO Organic/Inorganic Hybrids. Figure 2 depicts various sample schematics. Figure 2(a) shows a diazocine film drop-casted on FTO for the comparative characterizations. Figure 2(b) illustrates the morphology of bare ZnO NR array on FTO obtained by electron beam lithography and hydrothermal growth. ZnO NR bundles are situated 2 μm apart from each other and 1 μm tall. Figure 2(c) shows a structure of the organic/inorganic hybrid photoelectrode consisting of ZnO NR coated with the diazocine film which connects the ZnO NR bundles in between. Figure 2(d) shows a Pt NP-loaded diazocine film ZnO NR hybrid sample with the Pt NP acting as a cocatalyst to further enhance the photoelectrochemical performance.

Figure 3 shows the FESEM morphology characterization images. Figure 3(a) shows a diazocine film on FTO which fully covers the FTO substrate and shows the film uniformity. Figure 3(b) illustrates the structure of the inorganic ZnO NR array fabricated using electron-beam lithography. It shows that the ZnO NR branches are well-aligned. Figure 3(c) is a magnified image of the inorganic ZnO NR

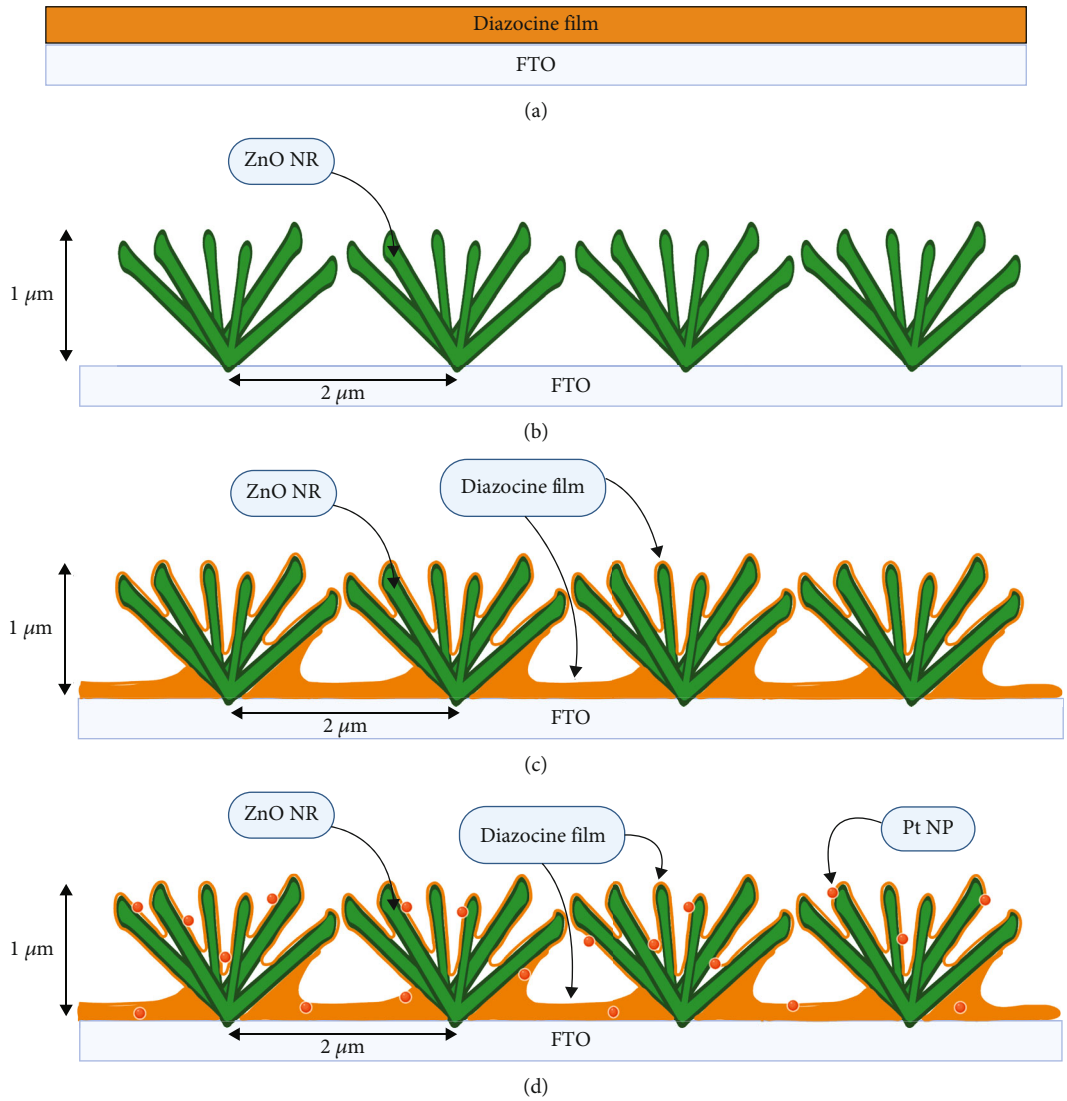

Figure 2: Schematic illustration of (a) diazocine film on FTO; (b) ZnO NR; (c) diazocine film/ZnO NR hybrid; and (d) diazocine film/ZnO NR/Pt NP hybrid.

array which shows a closer look at the ZnO NR bundle morphology and confirms that the center-to-center distance between the 1 μm tall ZnO NR bundles is 2 μm and that the inorganic brunches are well-aligned. Figure 3(d) shows a diazocine film/ZnO NR hybrid sample morphology where the conductive organic film covers the ZnO NRs and connects the ZnO NR bundles in between, allowing the charge transfer during the photoelectrochemical water-splitting reaction. The inset image in Figure 3(d) is a magnified picture of the hybrid sample which depicts a substantial organic film coverage on the inorganic ZnO NR. The ZnO NR bundle morphology allows a maximum contact area of the inorganic and organic counterparts which is beneficial for the efficiency of the photoanode. Figure 3(e) shows a Pt NP-loaded diazocine film/ZnO NR hybrid sample while Figure 3(f) is a magnified image of Pt NP-loaded organic/inorganic hybrid sample. Due to the fact that the Pt NPs were dispersed in the organic film solution before drop casting, it was a challenge to find distinct Pt NP using FESEM. Therefore, in order to observe the presence of catalyst NP, EDS-mapping characterization technique was used as shown in Figure 4.

A representative elemental mapping image of the Pt NP diazocine film/ZnO NR sample can be seen in Figure 4 depicting the presence and locations of Pt NPs in the organic sample on ZnO NR. As seen from Figure 4(a), the elemental-mapping image shows the presence of the Zn, O, C, and Pt elements on the FTO glass. As shown in Figure 4(b), carbon, which is the main component of the organic film, uniformly covers the ZnO NR inorganic sample. As seen from Figures 4(c) and 4(d), ZnO is mapped green on the image while Pt NP are mapped in red color dots. Therefore, even though it was a challenge to distinguish Pt NP in the film using FESEM, elemental map analysis confirmed the presence and distribution of the Pt NP in the hybrid sample.

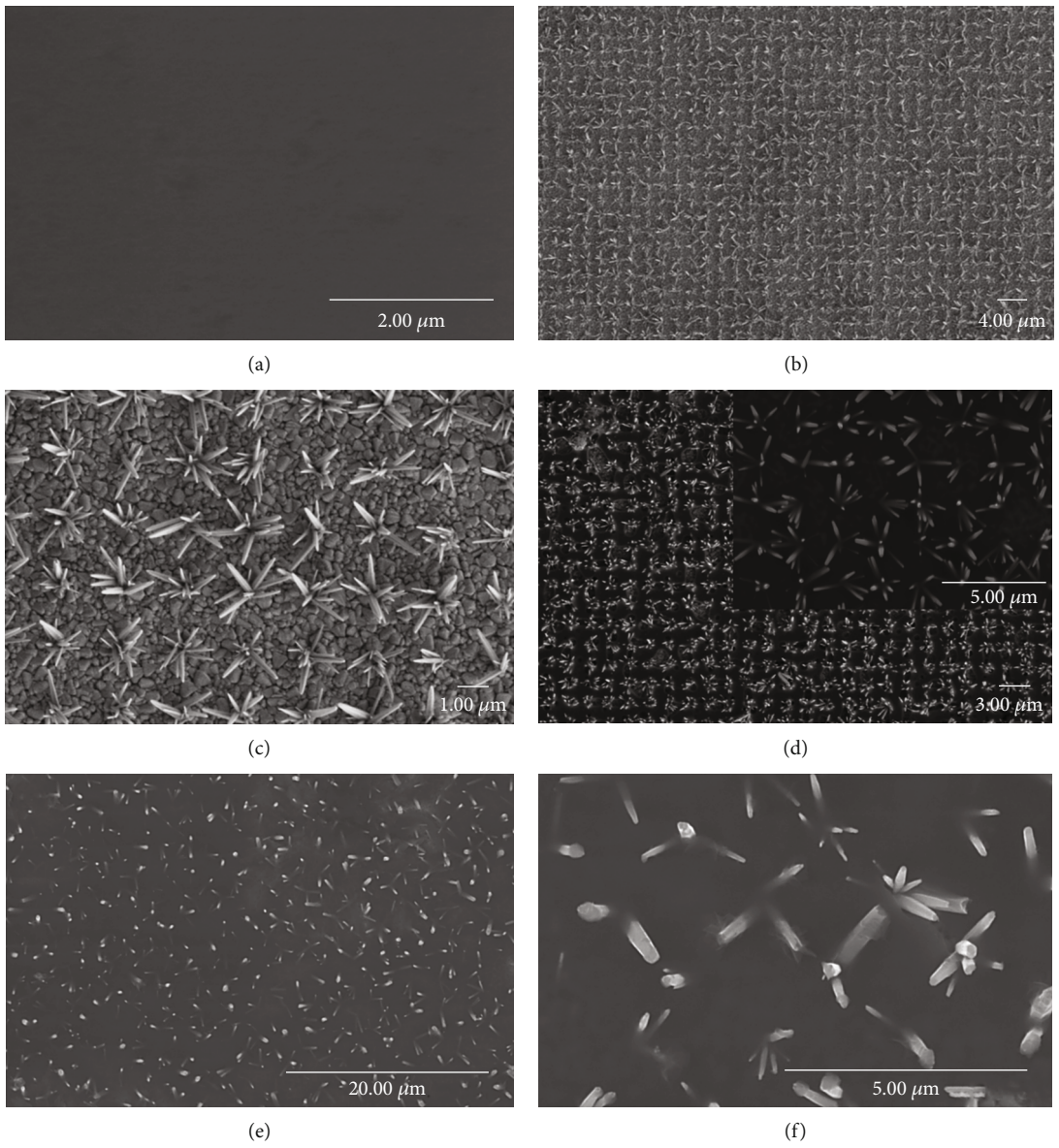

Figure 3: FESEM images of (a) diazocine film on FTO; (b) and (c) ZnO NR array; (d) diazocine film/ZnO NR hybrid; (e) diazocine film/ZnO NR/Pt NP hybrid; and (f) magnified diazocine film/ZnO NR/Pt NP hybrid.

3.3. Photochemical Behavior of Diazocine/ZnO Organic/Inorganic Hybrids. Figure 5(a) shows UV-visible absorbance spectra of ZnO NR and diazocine/ZnO NR hybrid with and without Pt NP catalyst. The main goal of the hybrid sample preparation is to widen the ultraviolet absorption edge and to enhance the absorption in visible spectra. As seen from the graph on Figure 5(a), hybrid organic/inorganic sample shows a red shift comparing to the bare ZnO sample and implies an absorbance expansion in ultraviolet range. Moreover, as can be observed, the diazocine film coated on ZnO NR boosts the absorption spectra in the visible light region which is highly desirable because the visible light accounts for 53% of the total solar spectrum which is a great portion while ultraviolet is only for 4% of solar spectrum. Therefore, even a minor enhancement in the visible light spectra is of a great significance for the efficiency advancement. Loading the hybrid sample with Pt NP further enhances the absorbance in visible light spectra allowing a better performance photoelectrode for solar water-splitting reaction.

The efficiency of trapping the charge and electron-hole recombination was observed by the means of photoluminescence measurements. Figure 5(b) demonstrates the quenching of photoluminescence spectra of ZnO NR, diazocine film, and hybrid sample in the range from 340 nm to 500 nm using a 266 nm excitation source. ZnO NR has the highest emission intensity at 380 nm while organic film's highest intensity is at 460 nm. However, when the hybrid sample is analyzed, the intensity of emission peak is decreased by 70% in comparison with the intensity peak for pristine ZnO NR implying that the recombination of

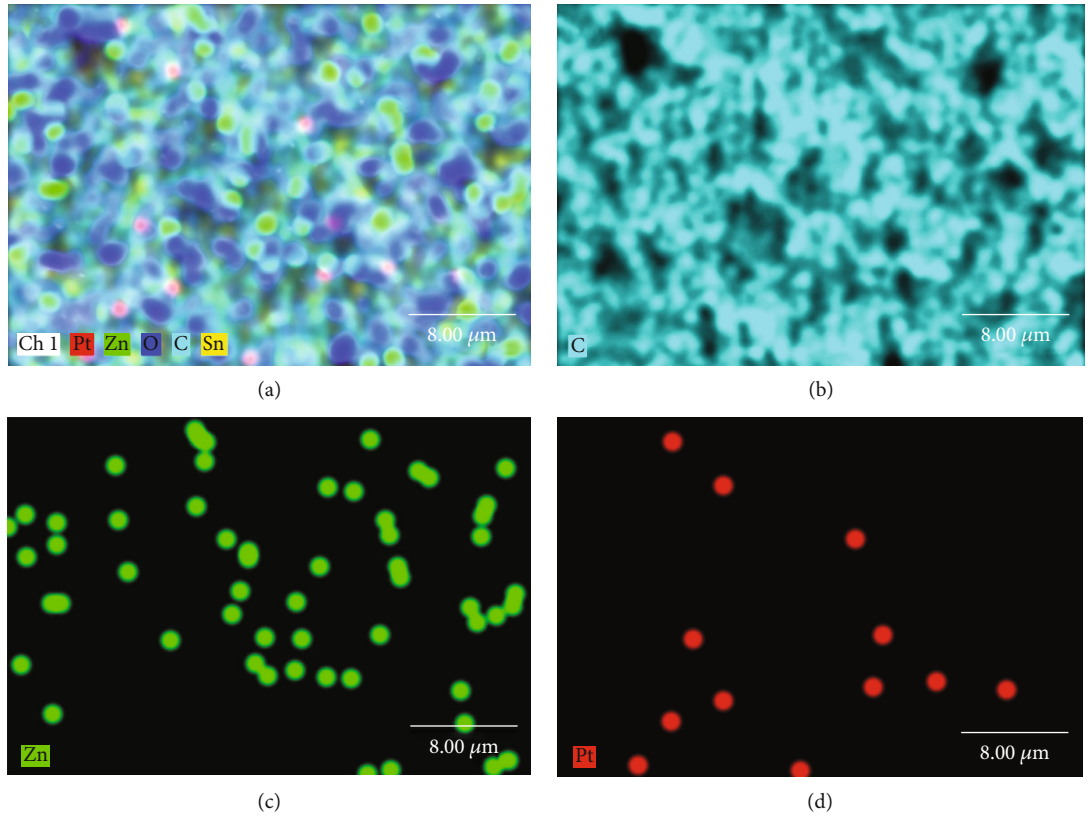

Figure 4: Elemental mapping of the Diazocine film/ZnO NR/Pt NP hybrid showing (a) distribution of the Zn, O, C, Sn and Pt elements throughout the given area; (b) organic C element distribution showing the uniformity of organic film coverage; (c) Zn elemental distribution and (d) cocatalyst Pt NP distribution.

charges was suppressed. Therefore, a water-splitting reaction is enhanced due to an effective charge transfer taking place through the photoanode and a greater number of charges available to participate in redox reactions.

To evaluate the performance of the prepared photoanode, linear sweep voltammograms were collected under 100 mW/cm^2-simulated solar light irradiation with AM 1.5 G, as shown in Figure 5(c). The pristine ZnO NR photocurrent measured in dark condition shows that the sample has a good reaction on solar light and was measured as a control for comparison with photocurrent under illumination. As observed from the photocurrent response graph of the prepared photoanodes, organic/inorganic diazocine/ZnO NR hybrid showed 1.256 mA/cm^2 at 1.23 V vs. RHE which is almost twice higher than the bare ZnO NR photoelectrode (0.716 mA/cm^2 at 1.23 V vs. RHE). This result correlated well with the UV-visible analysis and photoluminescence measurements. As such, the diazocine film enhances the photocatalytic activity of ZnO NR due to a red shift in ultraviolet spectra and increase in visible light photon absorbance. Moreover, the photocurrent is increased due to suppression of charge recombination and enhanced charge transfer mobility.

As seen from the J-V characteristic curve, loading the hybrid sample with the Pt NP cocatalyst further increases the current density value up to 1.636 mA/cm^2 at 1.23 V vs. RHE. As such, addition of Pt NP cocatalyst enhances the photocurrent value due to the increased number of active sites and surface area. One of the important points to highlight for the photocurrent response of organic/inorganic hybrid samples is that there is a gradual increase in photocurrent at first that can be attributed to the jumping of electrons from valence band to the conduction band till the saturation point. However, at about 1 V vs. RHE, the bump in peak can be observed. This implies that the photoexcited charges have moved from the valence band to the conduction band and a relative saturation point was achieved due to the maximum electron movement to the conduction band and saturation of the active sites on the surface of the photocatalyst. Therefore, it is observed that ohmic J-V curve for pristine ZnO originate in the original component while for the hybrid samples, a standard peak of the photoelectrochemical water-splitting reaction with its maximum saturation potential stabilization can be seen. This phenomenon shows an efficient electron-hole separation and charge transportation. Therefore, a synergistic effect of the branched array of ZnO NR structures with the diazocine film has an effect of improved charge separation and transfer properties along with the absorbance enhancement allowing a higher photocurrent production in photoelectrochemical water-splitting reaction.

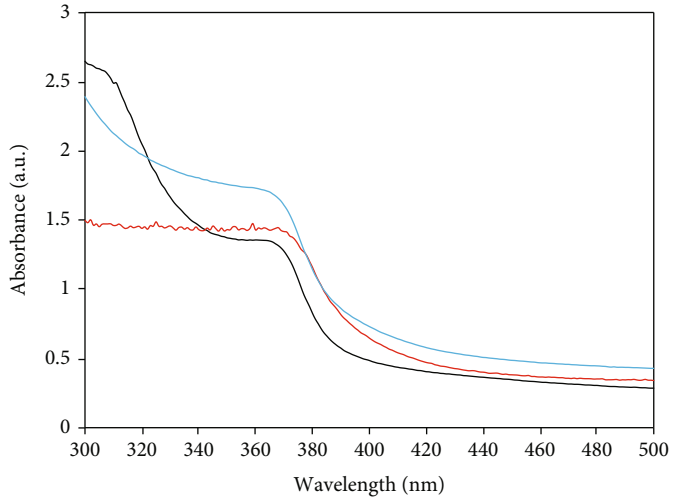

(a)

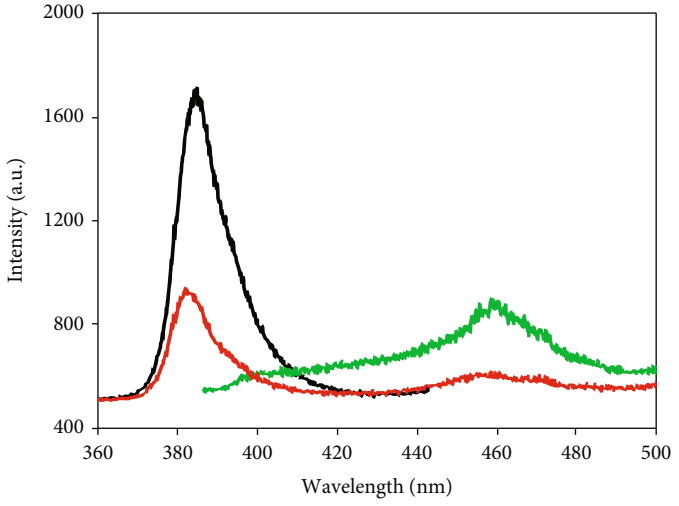

(b)

Figure 5: Continued.

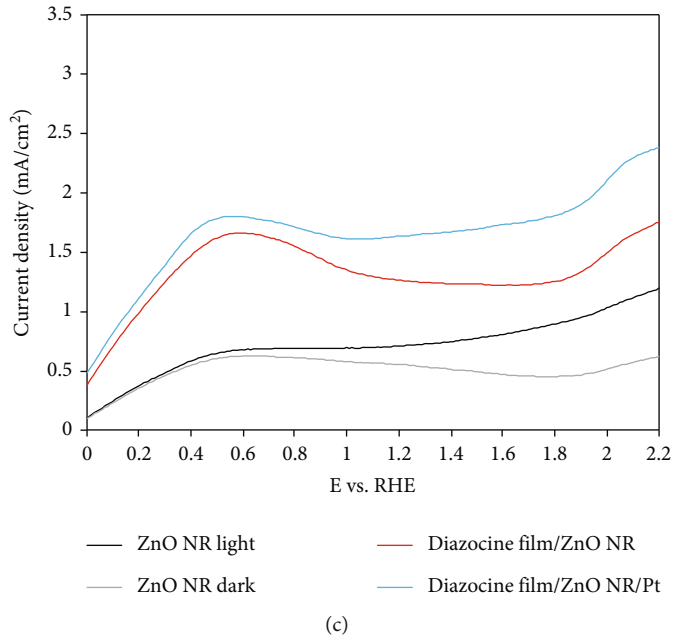

Figure 5: (a) Absorbance of ZnO NR, diazocine film/ZnO NR hybrid, and diazocine film/ZnO NR/Pt NP hybrid shows that diazocine film enhances the absorbance of ZnO NR; (b) photoluminescence spectra of ZnO NR, diazocine film, and diazocine film/ZnO NR hybrid excited by 266 nm laser; and (c) photocurrent J-V characteristic curves for the ZnO NR in dark and under illumination conditions, diazocine film/ZnO NR, and diazocine film/ZnO NR/Pt NP hybrid.

4. Conclusions

Dibenzo[b,f][1,5]diazocine derivatives exhibiting absorption in the visible light range were designed and synthesized to widen the absorption of ZnO NR arrays. Hybrid organic/inorganic nanosystem was prepared and its morphology was examined by FESEM. Optical properties were investigated by UV-visible absorbance showing that the hybrid sample has an enhanced light absorbance in visible spectra. The photoluminescence quenching was observed by PL measurements demonstrating the suppression of charge recombination and enhancement in carrier separation. The combination of these properties showed a significant increase in photocurrent density for the hybrid sample which accounts for 1.256 mA/cm^2, which is almost two times higher than for bare ZnO NR arrays (0.716 mA/cm^2 at 1.23 V vs. RHE). The addition of the Pt NP cocatalyst showed a further enhancement and increase in photocurrent density up to 1.636 mA/cm^2. Therefore, a hybrid organic/inorganic photoelectrode is a promising solution for the enhanced and more efficient solar water-splitting process which in its turn will contribute to more sustainable hydrogen production technologies and help in coping with a global climate problem.

Data Availability

All data used to support the findings of this study are included within the article.

Conflicts of Interest

The authors declare that they have no conflicts of interest.

Acknowledgments

This work was supported by a 2-Year Research Grant of Pusan National University.

References

[1] A. Kudo and Y. Miseki, "Heterogeneous photocatalyst materials for water splitting," *Chemical Society Reviews*, vol. 38, no. 1, pp. 253–278, 2009.

[2] M. G. Walter, E. L. Warren, J. R. McKone et al., "Solar water splitting cells," *Chemical Reviews*, vol. 110, no. 11, pp. 6446–6473, 2010.

[3] A. Fujishima and K. Honda, "Electrochemical photolysis of water at a semiconductor electrode," *Nature*, vol. 238, no. 5358, pp. 37-38, 1972.

[4] Y. Lin, G. Yuan, R. Liu, S. Zhou, S. W. Sheehan, and D. Wang, "Semiconductor nanostructure-based photoelectrochemical water splitting: a brief review," *Chemical Physics Letters*, vol. 507, no. 4-6, pp. 209–215, 2011.

[5] J. Joy, J. Mathew, and S. C. George, "Nanomaterials for photoelectrochemical water splitting - review," *International Journal of Hydrogen Energy*, vol. 43, no. 10, pp. 4804–4817, 2018.

[6] H. Ahmad, S. K. Kamarudin, L. J. Minggu, and M. Kassim, "Hydrogen from photo-catalytic water splitting process: a review," *Renewable and Sustainable Energy Reviews*, vol. 43, pp. 599–610, 2015.

[7] S. Rajaambal, K. Sivaranjani, and C. S. Gopinath, "Recent developments in solar H2 generation from water splitting," *Journal of Chemical Sciences*, vol. 127, no. 1, pp. 33–47, 2015.

[8] C. Jiang, S. J. A. Moniz, A. Wang, T. Zhang, and J. Tang, "Photoelectrochemical devices for solar water splitting – materials and challenges," *Chemical Society Reviews*, vol. 46, no. 15, pp. 4645–4660, 2017.

[9] K. Song, H. Hou, C. Gong et al., "Enhanced solar water splitting of BiVO4photoanodes byin situsurface band edge modulation," *Journal of Materials Chemistry A*, vol. 10, no. 42, pp. 22561–22570, 2022.

[10] D. Chandra, K. Saito, T. Yui, and M. Yagi, "Crystallization of tungsten trioxide having small mesopores: highly efficient photoanode for visible-light-driven water oxidation," *Angewandte Chemie, International Edition*, vol. 52, no. 48, pp. 12606–12609, 2013.

[11] Z. Ma, K. Song, L. Wang et al., "WO3/BiVO4 type-II heterojunction arrays decorated with oxygen-deficient ZnO passivation layer: a highly efficient and stable photoanode," *ACS Applied Materials & Interfaces*, vol. 11, pp. 889–897, 2018.

[12] B. Moss, O. Babacan, A. Kafizas, and A. Hankin, "A review of inorganic photoelectrode developments and reactor scale-up challenges for solar hydrogen production," *Advanced Energy Materials*, vol. 11, no. 13, article 2003286, 2021.

[13] Z. Luo, T. Wang, and J. Gong, "Single-crystal silicon-based electrodes for unbiased solar water splitting: current status and prospects," *Chemical Society Reviews*, vol. 48, no. 7, pp. 2158–2181, 2019.

[14] S. S. Yi, X. B. Zhang, B. R. Wulan, J. M. Yan, and Q. Jiang, "Non-noble metals applied to solar water splitting," *Energy & Environmental Science*, vol. 11, no. 11, pp. 3128–3156, 2018.

[15] S. Singh, H. Chen, S. Shahrokhi et al., "Hybrid organic–inorganic materials and composites for photoelectrochemical water splitting," *ACS Energy Letters*, vol. 5, pp. 1487–1497, 2020.

[16] P. Ruankham, L. Macaraig, T. Sagawa, H. Nakazumi, and S. Yoshikawa, "Surface modification of ZnO nanorods with small organic molecular dyes for polymer-inorganic hybrid solar cells," *Journal of Physical Chemistry C*, vol. 115, no. 48, pp. 23809–23816, 2011.

[17] W. Cui, H. Bai, J. Shang et al., "Organic-inorganic hybrid-photoanode built from NiFe-MOF and TiO_2 for efficient PEC water splitting," *Electrochimica Acta*, vol. 349, article 136383, 2020.

[18] D. Shao, Y. Cheng, J. He et al., "A spatially separated organic–inorganic hybrid photoelectrochemical cell for unassisted overall water splitting," *ACS Catalysis*, vol. 7, pp. 5308–5315, 2017.

[19] D. Jeon, N. Kim, S. Bae, Y. Han, and J. Ryu, "WO3/conducting polymer heterojunction photoanodes for efficient and stable photoelectrochemical water splitting," *ACS Applied Materials & Interfaces*, vol. 10, no. 9, pp. 8036–8044, 2018.

[20] L. Wang, D. Yan, D. W. Shaffer et al., "Improved stability and performance of visible photoelectrochemical water splitting on solution-processed organic semiconductor thin films by ultrathin metal oxide passivation," *Chemistry of Materials*, vol. 30, no. 2, pp. 324–335, 2018.

[21] M. Szkoda, J. Rysz, J. Ryl, A. Lisowska-Oleksiak, and K. Siuzdak, "Fabrication and photoactivity of organic-inorganic systems based on titania nanotubes and PEDOT containing redox centres formed by different Prussian blue analogues," *Journal of Alloys and Compounds*, vol. 723, pp. 498–504, 2017.

[22] Y. Jia, P. Xiao, H. He et al., "Photoelectrochemical properties of polypyrrole/TiO_2 nanotube arrays nanocomposite under visible light," *Applied Surface Science*, vol. 258, no. 17, pp. 6627–6631, 2012.

[23] S. K. Cho, J. H. Jung, Y. Sissembayeva, J. H. Song, D. I. Jung, and Y. H. Hwang, "Microwave assisted synthesis of dibenzo-[b,f][1,5]diazocine derivatives for photocatalytic water splitting applications," *Chemistry, an Asian Journal*, vol. 33, no. 3, pp. 627–631, 2021.